Splicing function of mitotic regulators links R-loop–mediated DNA damage to tumor cell killing

Yihan Wan,[1,2] Xiaobin Zheng,[2] Haiyang Chen,[2] Yuxuan Guo,[2] Hao Jiang,[1,2] Xiaonan He,[1] Xueliang Zhu,[1] and Yixian Zheng[2]

[1]State Key Laboratory of Cell Biology, Institute of Biochemistry and Cell Biology, Shanghai Institutes for Biological Sciences, Chinese Academy of Sciences, Shanghai 200031, China
[2]Department of Embryology, Carnegie Institution for Science, Baltimore, MD 21218

Although studies suggest that perturbing mitotic progression leads to DNA damage and p53 activation, which in turn lead to either cell apoptosis or senescence, it remains unclear how mitotic defects trigger p53 activation. We show that BuGZ and Bub3, which are two mitotic regulators localized in the interphase nucleus, interact with the splicing machinery and are required for pre-mRNA splicing. Similar to inhibition of RNA splicing by pladienolide B, depletion of either BuGZ or Bub3 led to increased formation of RNA–DNA hybrids (R-loops), which led to DNA damage and p53 activation in both human tumor cells and primary cells. Thus, R-loop–mediated DNA damage and p53 activation offer a mechanistic explanation for apoptosis of cancer cells and senescence of primary cells upon disruption of the dual-function mitotic regulators. This demonstrates the importance of understanding the full range of functions of mitotic regulators to develop antitumor drugs.

Introduction

Extensive studies have shown that prolonged mitotic arrest can lead to DNA damage and p53 activation. Although p53 activation in these cells would explain why targeting mitotic regulators could be effective for cancer therapy (Lanni and Jacks, 1998; Quignon et al., 2007; Huang et al., 2010; Uetake and Sluder, 2010; Orth et al., 2012), how mitotic arrest leads to DNA damage and p53 activation is not fully understood in some contexts. For example, prolonged mitosis is proposed to cause DNA or cellular damage that would in turn activate p53 (Quignon et al., 2007; Ganem and Pellman, 2012; Hayashi et al., 2012). Supporting this idea, prolonged mitotic arrest has been shown to cause Caspase activation, which could activate CAD (Caspase-activated DNase). Although CAD could lead to DNA damage and p53 activation (Gascoigne and Taylor, 2008; Orth et al., 2012), how prolonged mitosis activates Caspases is not clear in this context. Additionally, mitotic timer has been suggested to sense the prolonged mitotic arrest in either a p53-dependent or independent manner (Blagosklonny, 2006; Inuzuka et al., 2011; Wertz et al., 2011). While a p53-dependent timer could link prolonged mitotic block to p53 activation, neither the nature of this timer nor the signal that activates p53 has been defined in these settings.

The difficulty in defining the mitotic trigger for DNA damage and p53 activation could be because we have not looked at the right stage of the cell cycle. Indeed, several mitotic regulators are found in the interphase nucleus. Therefore, p53 activation could be caused by the disruption of the interphase nuclear functions of these mitotic regulators. Recently, a nuclear zinc finger protein BuGZ has been shown to regulate mitosis by directly binding to the spindle assembly checkpoint protein Bub3 to promote its loading to kinetochores and chromosome alignment (Jiang et al., 2014; Toledo et al., 2014). Interestingly, Bub3 is also localized to the interphase nucleus, and the interaction between BuGZ and Bub3 can be detected throughout the cell cycle. As expected, BuGZ depletion in various cancer cell lines resulted in a great reduction in the kinetochore Bub3 levels, chromosome misalignment, and mitotic block. Curiously, upon a prolonged mitotic block, most of the BuGZ-depleted tumor cells undergo mitotic death (mitotic catastrophe). By investigating this mitotic catastrophe phenomenon, we have uncovered an unrecognized interphase

Correspondence to Yixian Zheng: zheng@ciwemb.edu; or Xueliang Zhu: xlzhu@sibcb.ac.cn

Abbreviations used in this paper: HFF, human foreskin fibroblast; SA-β-gal, senescence-associated β-gal.

The Rockefeller University Press $30.00
J. Cell Biol. Vol. 209 No. 2 235–246
www.jcb.org/cgi/doi/10.1083/jcb.201409073

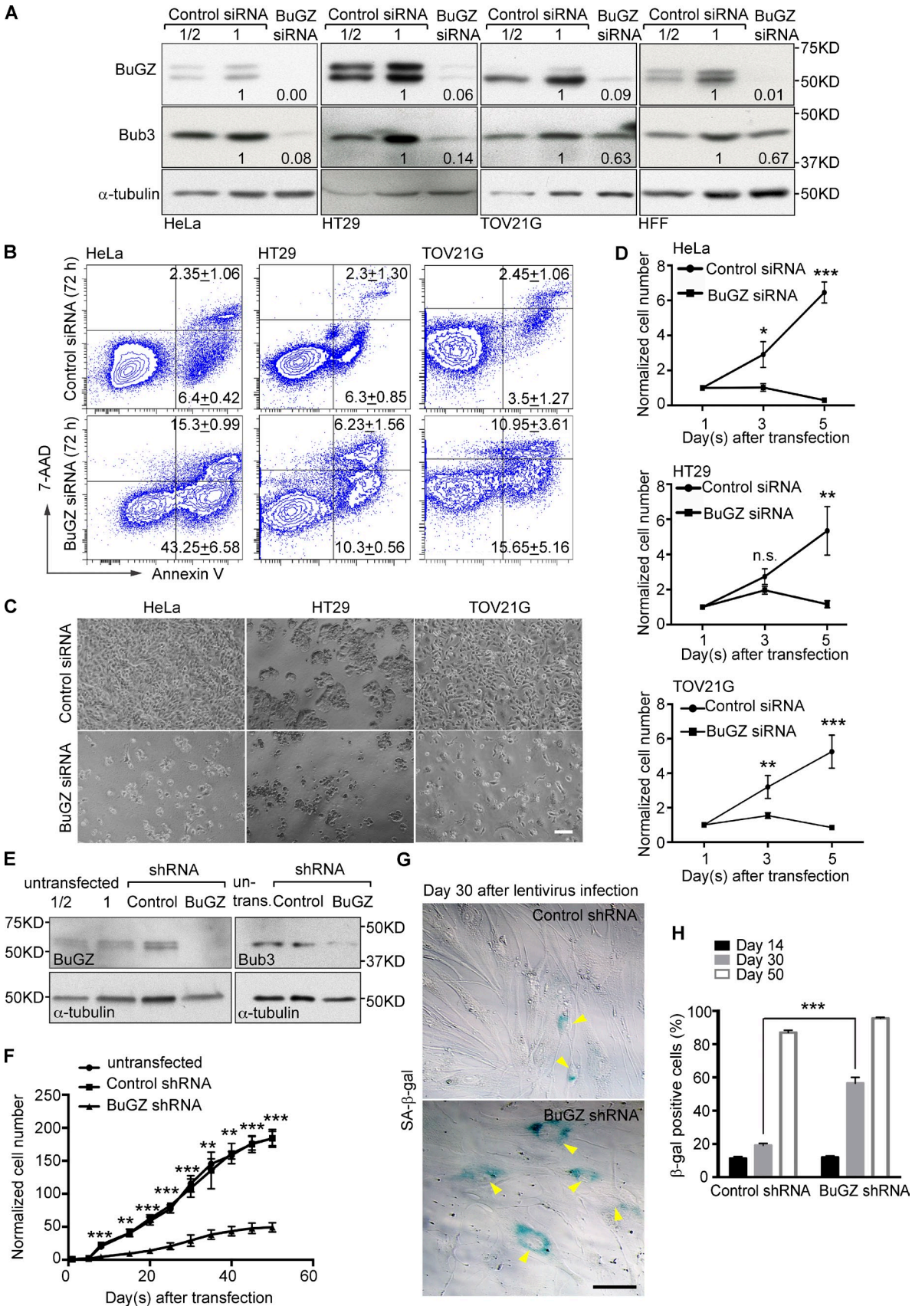

Figure 1. **Reduction of BuGZ causes apoptosis in human cancer cells but senescence in primary foreskin fibroblasts (HFFs).** (A) Depletion of BuGZ by siRNA treatment in the indicated cells. Two different amounts of control lysates (1/2 or 1) were loaded. Cells were analyzed 60 h after siRNAs transfection. α-tubulin, loading control. The numbers at the bottom of each lane indicate relative levels of BuGZ or Bub3 compared with controls, which were set to 1.

nuclear function of BuGZ and Bub3. This interphase function helps to explain why the disruption of the two mitotic regulators could lead to p53 activation.

Results and discussion

Depletion of BuGZ causes apoptosis in cancer cells and senescence in primary fibroblasts

Previous studies have shown that BuGZ depletion in cancer cells destabilizes Bub3 and causes chromosome misalignment and mitotic arrest followed by massive cell death (Jiang et al., 2014; Toledo et al., 2014). To further study the function of BuGZ, we used siRNA to deplete the protein in three cancer cell lines (HeLa, HT29, or TOV21G) and the primary human foreskin fibroblasts (HFFs). Consistent with the role of BuGZ in maintaining Bub3 protein level, BuGZ depletion in these cells by 60 h of siRNA treatment led to Bub3 reduction (Fig. 1 A) and an elevation of mitotic index (Fig. S1 A). This shows that BuGZ is required for efficient chromosome alignment in both cancer cells and HFFs, as would be expected based on the Bub3 reduction upon BuGZ depletion.

By 5 d of the siRNA treatment, all three cancer cell lines exhibited a large increase in apoptosis as judged by the early and late apoptotic markers Annexin V and 7-AAD, respectively (Fig. 1 B), which correlated with a striking reduction in cell numbers (Fig. 1, C and D). In contrast, BuGZ siRNA treatment of HFFs did not affect cell survival (Fig. S1 B), which is similar to the observation in primary neural stem cells (Toledo et al., 2014), despite a moderate elevation in mitotic index (Fig. S1 A). Nevertheless, because primary somatic cells usually grow more slowly than tumor cells, we reasoned that a time >5 d might be required for properly assessing the effect of BuGZ depletion on HFFs. We thus used lentivirus-mediated RNAi to stably knock down BuGZ in HFFs (Fig. 1 E). We found that, from day 8 after infection, the proliferation rate of the BuGZ-RNAi HFFs began to significantly slow down (Fig. 1 F). Moreover, a threefold increase of senescent cells was observed at 30 d compared with controls (Fig. 1, G and H), which indicates accelerated senescence of BuGZ-depleted HFFs. Thus, BuGZ depletion causes apoptosis in cancer cells and senescence in primary HFFs.

Depletion of BuGZ leads to p53 activation

Since p53 accumulation is known to cause either apoptosis or senescence depending on the cellular context (Surova and Zhivotovsky, 2013; Khoo et al., 2014), we asked whether BuGZ depletion led to p53 induction in cancer cells and HFFs. HeLa and TOV21G cells have wild-type p53 (Forbes et al., 2011). Although in HeLa cells p53 protein is targeted for degradation by the human papillomavirus E6 proteins under normal conditions (Scheffner et al., 1990), its accumulation has been reported upon DNA damage or oxidation (Chen et al., 2002; Ismail et al., 2005; Porameesanaporn et al., 2013). HT29 cells have a point mutation in the transactivation domain of p53 (R273H), but studies have shown that this mutant p53 induces apoptosis or cell cycle arrest upon various challenges (Stähler and Roemer, 1998; Song et al., 2005). Activation of p53 in primary cells with intact cell cycle checkpoints has been shown to cause senescence (Campisi and d'Adda di Fagagna, 2007). Consistently, we found that the levels of total p53 and activated p53 (phospho-p53 at serine 15) were increased upon BuGZ depletion in both the cancer cells tested and HFFs (Fig. 2, A and B).

Our previous studies indicated that many BuGZ-depleted HeLa cells initially arrested in mitosis and then underwent cell death (Jiang et al., 2014). To test whether p53 activation could be the cause of cancer cell death, we treated cells with p53 inhibitor PFT-α (Komarov et al., 1999) 12 h after transfection of control or BuGZ siRNA and found that the inhibition of p53 significantly rescued the cell number reduction of the BuGZ-depleted cancer cells (Fig. 2 C). When HFFs were coinfected with lentivirus to express p53 shRNA, senescence induced by BuGZ depletion upon prolonged culturing was also significantly inhibited (Fig. 2, D–F). Because depletion of BuGZ down-regulated Bub3 (Fig. 1 A; Jiang et al., 2014; Toledo et al., 2014), we investigated whether Bub3 reduction could also lead to p53 activation. We found that knockdown of Bub3 by RNAi caused prominent p53 accumulation and activation in both cancer cells and HFFs (Fig. S1, C–F). These findings show that p53 mediates both apoptosis in cancer cells and senescence in HFFs upon BuGZ depletion.

BuGZ and Bub3 are required for proper pre-mRNA splicing

Next we explored how the depletion of BuGZ or Bub3 could activate p53. Because BuGZ and Bub3 bind to one another and are both present in the interphase nucleus (Jiang et al., 2014; Toledo et al., 2014), their depletion could disrupt an interphase nuclear function, which in turn might trigger p53 activation. To investigate this, we examined our previous proteome analyses of BuGZ-interacting proteins (Jiang et al., 2014). Besides Bub3, we noticed several spliceosome components among the top candidates of BuGZ-interacting proteins (Fig. 3 A). Among a number of available antibodies to spliceosome components, we found that the antibodies to two—U2AF65 and SF3a3—worked in both immunoprecipitation and Western blotting, which allowed us to use reciprocal

Note that >90% of BuGZ was depleted by RNAi. (B) FACS assays for the quantification of apoptotic cells at 72 h after RNAi. Early apoptotic cells were Annexin V positive (see the bottom right quadrants), whereas late apoptotic ones were Annexin V and 7-aminoactinomycin D (7-AAD) double positive (the top right quadrants). All values are percentages of total cells, presented as mean ± SD from three independent experiments. (C) Representative microscopic fields of cells at 72 h after RNAi. Bar, 100 µm. (D) Growth curves of cells treated with control or BuGZ siRNA. Error bars indicate SD. Student's *t* test: n.s., not significant; *, $P < 0.05$; **, $P < 0.01$; ***, $P < 0.001$ from three independent experiments. (E) Stable knockdown of BuGZ with lentivirus-expressed shRNA in HFFs. The virus-infected cells were enriched by puromycin selection. The cell lysates were collected at day 5. (F) Growth curves of HFFs at the indicated days after shRNA transfection. Error bars indicate SD. Student's *t* test: **, $P < 0.01$; ***, $P < 0.001$ from three independent experiments. (G) Increased senescence in BuGZ shRNA-transfected HFFs as judged by SA-β-gal staining (arrowheads). Bar, 50 µm. (H) Percentage of SA-β-gal–positive cells at the indicated days after shRNA transfection. Error bars indicate SEM. Student's *t* test: ***, $P < 0.001$ from three independent experiments.

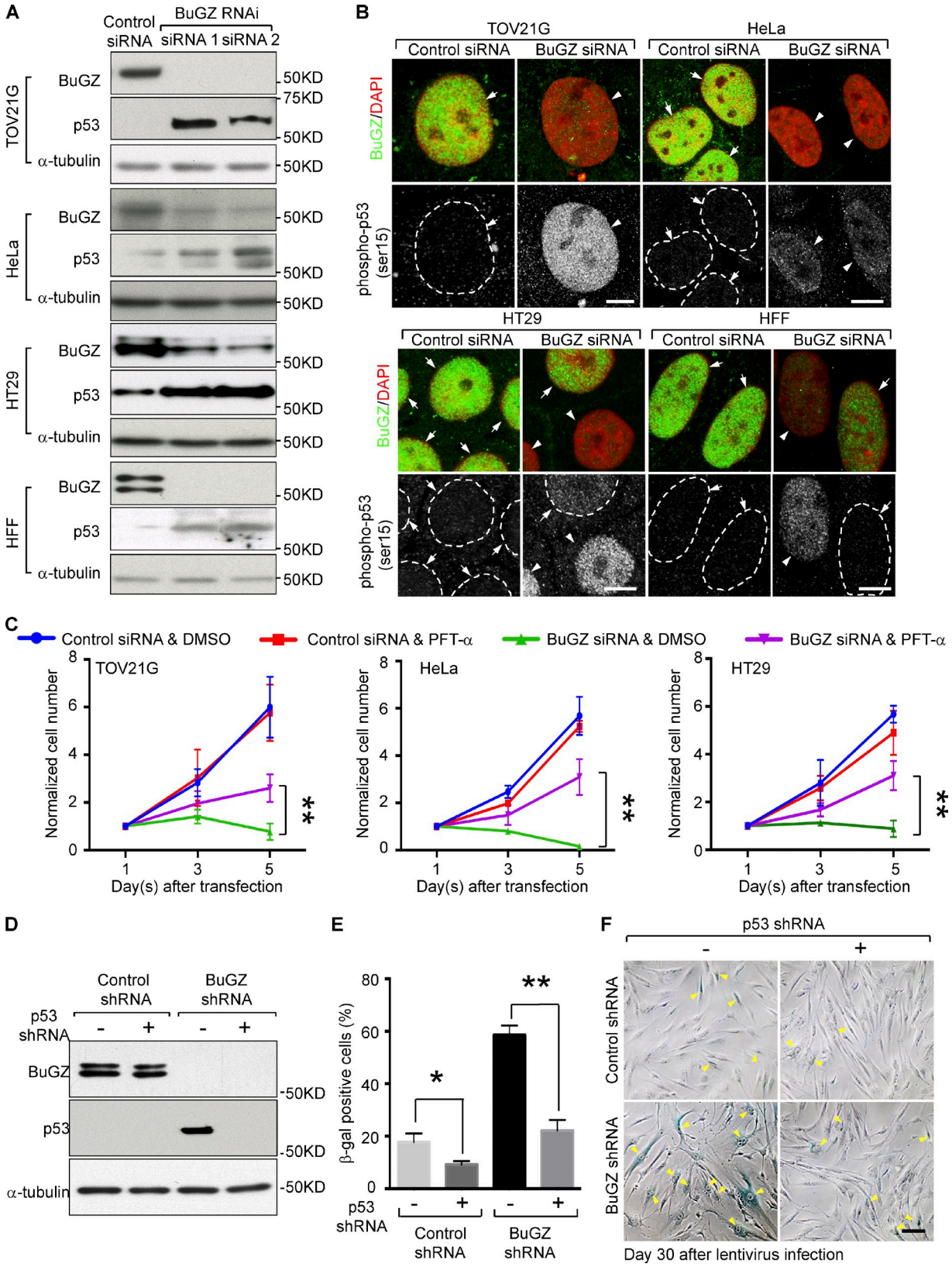

Figure 2. **Activation of p53 upon BuGZ depletion leads to apoptosis or senescence.** (A) Up-regulation of p53 after 48 h of BuGZ siRNA treatment. Loading control, α-tubulin. (B) Increased phospho-p53 (Ser15) in the nuclei of BuGZ-depleted cells (arrowheads). BuGZ-positive (arrows) and phospho-p53 negative cells (arrows and white broken circles) are indicated. Cells were assayed 48 h after siRNA treatment. Bars, 10 µm. (C) Inhibition of p53 by PFT-α increased the numbers of viable BuGZ-depleted cells. Error bars indicate SD. Student's *t* test: **, $P < 0.01$ from three independent experiments. (D–F) p53 RNAi in HFFs repressed senescence induced by BuGZ knockdown. HFFs were infected with lentivirus to express the indicated shRNAs. Western blotting (D) and quantification (E) of SA-β-gal staining (F) were performed at 30 d after infection. Arrowheads in F represent the SA-β-gal–positive staining cells. Bar, 100 µm. Error bars indicate SEM. Student's *t* test: *, $P < 0.05$; **, $P < 0.01$ from three independent experiments.

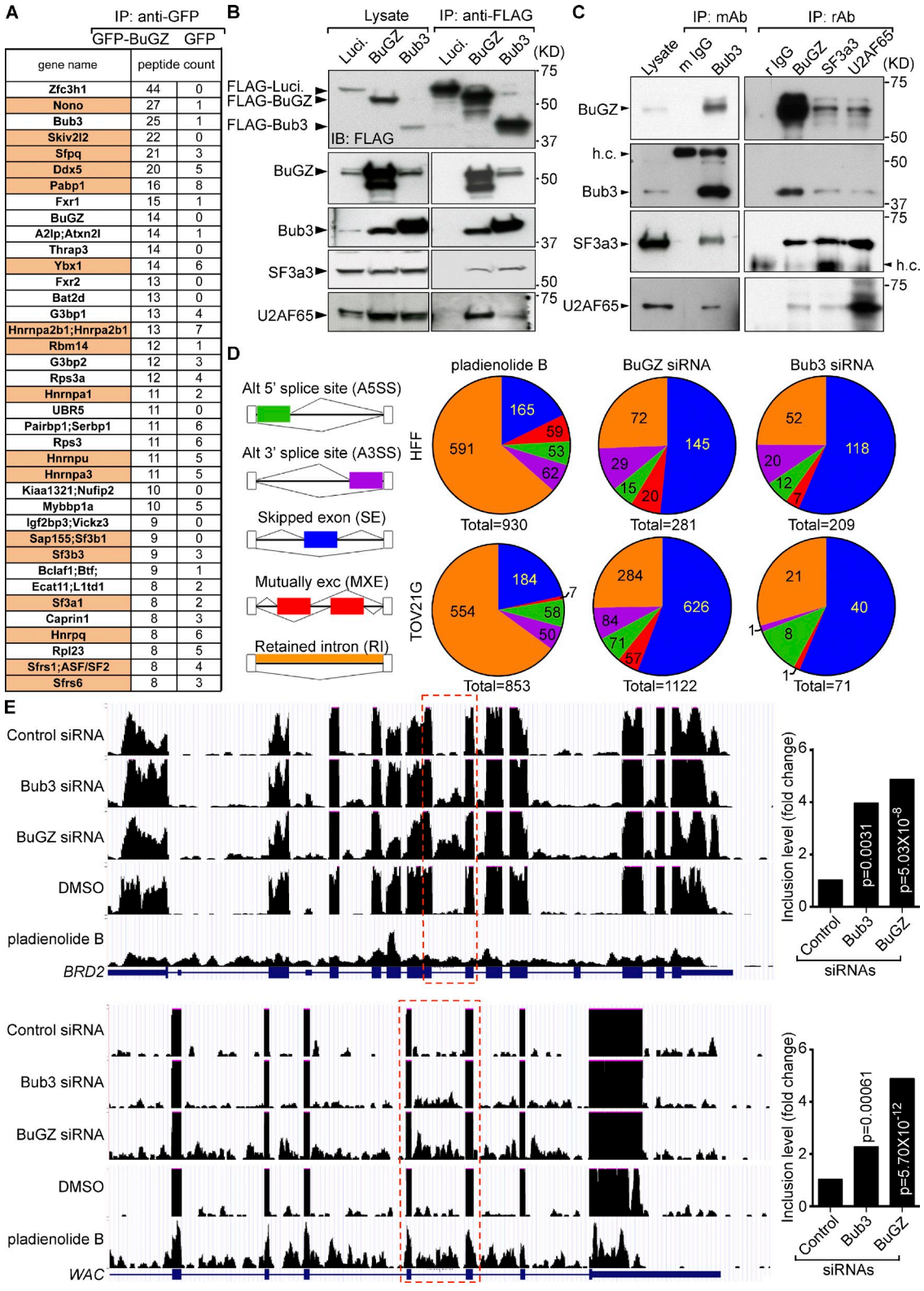

Figure 3. **A requirement of BuGZ and Bub3 for RNA splicing.** (A) Proteins with known functions in RNA splicing (highlighted in orange) were found as candidate BuGZ-interacting proteins. (B) FLAG-tagged BuGZ or Bub3, but not FLAG-luciferase (Luci.), immunoprecipitated the spliceosome components SF3a3 and U2AF65 in HEK293T cells. (C) BuGZ and Bub3 interacted with SF3a3 and U2AF65 in vivo. Reciprocal immunoprecipitations of endogenous proteins were performed using HT29 cell lysates with the indicated mouse monoclonal (mAb) or rabbit antibodies (rAb). h.c., antibody heavy chain. Experiments were performed three times. (D) Analyses of splicing defects by RNA-sequencing of HFFs and TOV21G cells treated by the splicing inhibitor pladienolide B or RNAi of BuGZ or Bub3. The numbers of genes exhibiting the depicted splicing defects are shown as pie charts. RNA-Seq was from two biological repeats. (E) Two representative genes, *BRD2* and *WAC*, exhibiting intron retention upon treatment with pladienolide B or RNAi of BuGZ or Bub3. The red boxes highlight examples of intron retention. The fold increases of the intron retention are plotted to the right. The p-values were generated by simulation (MATS: a Bayesian framework for flexible detection of differential alternative splicing from RNA-Seq data).

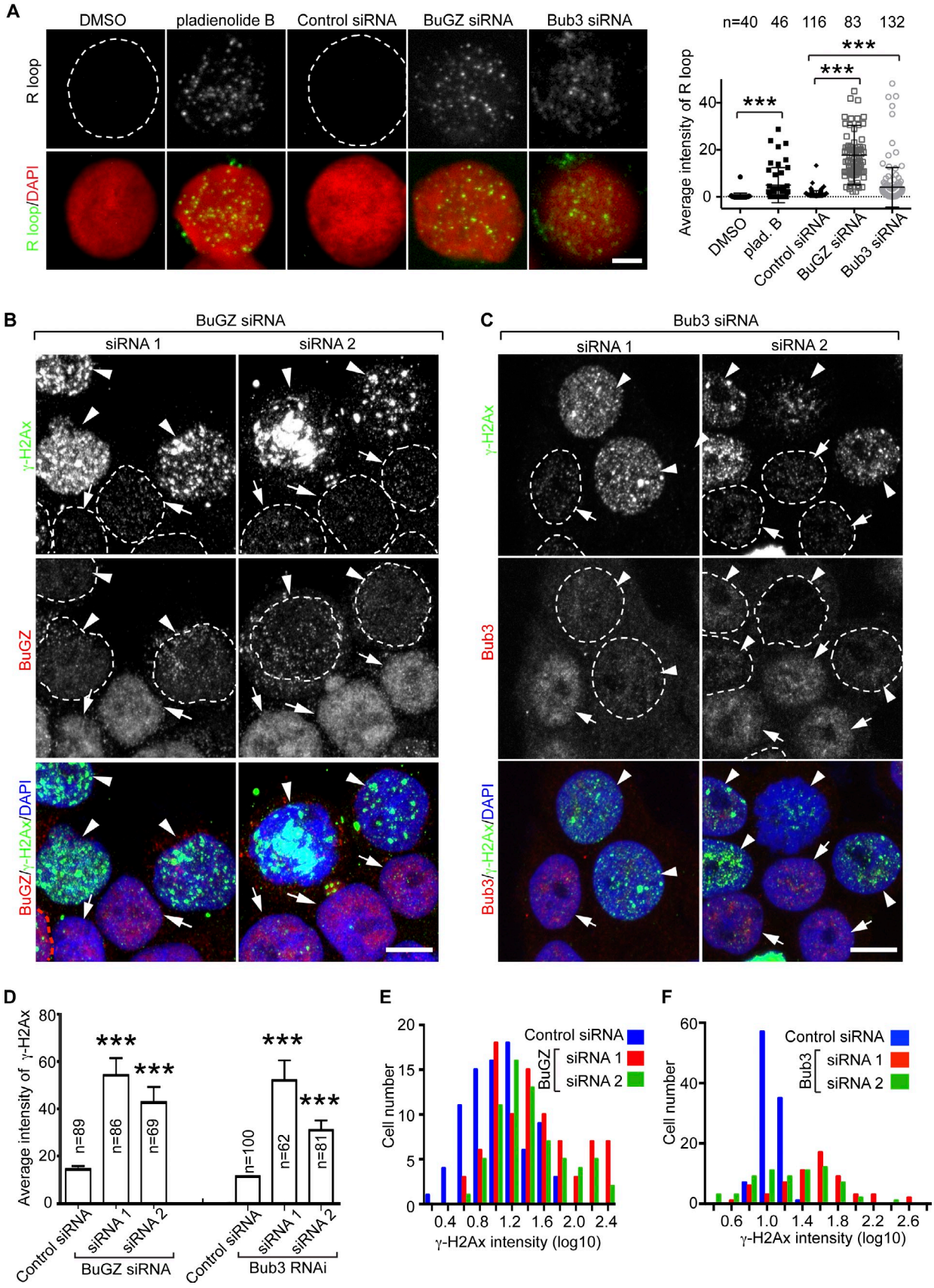

Figure 4. **Depletion of BuGZ or Bub3 leads to increased R-loop formation and DNA damage.** (A) Depletion of BuGZ or Bub3 resulted in increased R-loop formation in HT29 cells. Pladienolide B treatment was used as a positive control. White broken circles outline the nuclei with no or low levels of R-loops. Bar, 5 µm. The quantification of mean fluorescence intensity of the R-loop is shown on the right. Student's *t* test: ***, P < 0.001 from three independent

immunoprecipitation to provide further support for an interaction between BuGZ/Bub3 and the spliceosome (Fig. 3, B and C). Consistently, both BuGZ and Bub3 have also been found in previous proteomic analyses of spliceosomes (Wahl et al., 2009; Hegele et al., 2012).

To test whether BuGZ and Bub3 play roles in splicing, we depleted each protein in cancer cells (TOV21G) or HFFs and performed RNA sequencing (accession number: GSE67770). Cells treated with pladienolide B, a potent splicing inhibitor (Kotake et al., 2007; Effenberger et al., 2013), were used as positive controls. Among the splicing defects depicted in Fig. 3 D, we found that the depletion of either Bub3 or BuGZ mainly caused exon skipping, whereas pladienolide B treatment mainly resulted in intron retention (Fig. 3, D and E; and Table S1). The difference in the resultant splicing defects between Pladienolide B inhibition (which targets SF3b3) and BuGZ or Bub3 depletion suggests that BuGZ and Bub3 function differentially from SF3b3. Whereas further studies are required to understand how BuGZ and Bub3 regulate splicing, these analyses show that the well-established SAC component Bub3 and its regulator BuGZ also play roles in interphase RNA splicing. Depletion of BuGZ in transformed cells (Jiang et al., 2014; Toledo et al., 2014) or treatment of tumor cells with pladienolide B (Sato et al., 2014) have been shown to kill these cells in vitro. Interestingly, using the *Drosophila melanogaster* eye tumor model (Gonzalez, 2013), we found that the eye hyperproliferation induced by the activation of either the *Jak-Stat* or the *Hippo* (unpublished data) pathway was inhibited by the eye-specific BuGZ RNAi or by feeding the flies with pladienolide B (Fig. S2 A).

Depletion of BuGZ or Bub3 causes R-loop formation and DNA damage

Deficiency in RNA splicing has been shown to cause an increased formation of RNA–DNA hybrids (R-loops) in the nucleus, and subsequent DNA breaks and p53 activation (Li and Manley, 2005; Paulsen et al., 2009; Lin et al., 2010; Gan et al., 2011; Wahba et al., 2011; Aguilera and García-Muse, 2012; Wongsurawat et al., 2012). Therefore, p53-mediated killing of transformed cells or senescence of primary cells as we observed in the above studies could be caused by defects in splicing and the subsequent R-loop formation. To determine whether cells depleted of BuGZ or Bub3 had an increased R-loop formation, we used the monoclonal antibody S9.6, which recognizes RNA–DNA hybrids (Phillips et al., 2013). Similar to the pladienolide B treatment (Fig. 4 A), depletion of BuGZ or Bub3 markedly stimulated R-loop formation in both cancer cells and HFFs (Fig. 4 A and Fig. S2, B and C). These cells also exhibited increased DNA damage, as judged by the appearance of prominent nuclear foci of γH2AX (Pilch et al., 2003; Fig. 4, B–F; Fig. S2, D–H; and Fig. S3 A). These results suggest that defects in the splicing function of BuGZ and Bub3 lead to R-loop–induced DNA damage, which in turn contributes to p53 activation.

Inhibition of R-loop formation attenuates p53 activation and DNA damage caused by depletion of BuGZ or Bub3

To confirm that the R-loops formed in cells depleted of BuGZ or Bub3 indeed contributed to DNA damage and p53 activation, we used a modified form of RNase H1 lacking the mitochondria targeting sequence (Cerritelli et al., 2003). This form of RNase H1 has been shown to localize only in the nucleus and to resolve R-loops (Drolet et al., 1995; Lin et al., 2010; Wahba et al., 2011; Wimberly et al., 2013; Groh et al., 2014). By analyzing the nuclei that were positive for the GFP-tagged RNase H1 or GFP control, we found that expression of the enzyme resulted in significant reduction of both γH2AX foci (Fig. 5, A–C) and p53 activation (Fig. 5, D–F) in BuGZ-depleted HT29 cells. A similar effect of RNase H1 was also observed in pladienolide B–treated (Fig. S3 B) or Bub3-depleted (Fig. 5, G–J) HT29 cells. The inability of RNase H1 to fully rescue DNA damage and p53 activation could be caused by the heterogeneous level of GFP-RNase H1 expression, the inefficiency of GFP-RNase H1 to resolve certain R-loops, or other uncharacterized defects. Nonetheless, these findings show that R-loop formation due to the disruption of the splicing function of Bub3 and BuGZ (Fig. S3 C) contributes to DNA damage and p53 activation.

Extensive efforts have been devoted to understanding how mitotic arrest as a result of disrupting mitotic regulators can lead to p53-dependent cell death or cell cycle arrest in cancer cells. By exploring the mitosis-independent functions, we have uncovered a critical role of the mitotic regulators BuGZ and Bub3 in interphase RNA splicing. Importantly, we demonstrated that disruption of this interphase function by depleting BuGZ or Bub3 leads to R-loop formation, DNA damage, and p53 activation. Furthermore, our results suggest that the splicing inhibitor pladienolide B, a potent anticancer reagent (Kotake et al., 2007; Eskens et al., 2013; Sato et al., 2014), kills cancer cells through a similar mechanism. Our findings demonstrate that by looking beyond the mitosis functions of the established mitotic regulators, we could gain significant insights into how aberrant mitosis is connected to the suppression of cell proliferation and the safeguard of genome stability. Therefore, a broadened understanding of the function of mitotic regulators beyond cell division should facilitate the selection of therapeutic targets in the effort of developing new antitumor drugs for cancer chemotherapy.

Materials and methods

For the sources and sequences of mammalian expression plasmids, antibodies (with dilutions used), siRNA, shRNA, small molecules (with concentrations

experiments. (B and C) Depletion of BuGZ (B) or Bub3 (C) by two different siRNAs in HT29 cells caused increased DNA damage, as judged by the presence of prominent nuclear foci of γ-H2Ax. BuGZ- or Bub3-depleted cells (arrowheads) exhibit more γ-H2Ax foci than cells with insufficient or no depletion (arrows). White broken circles outline the nuclei. Bars, 10 µm. (D–F) Quantification of γ-H2Ax intensities in individual cells (D) and distributions of γ-H2Ax intensities (E and F). Error bars indicate SEM. Student's *t* test: ***, $P < 0.001$. Cell numbers (*n*) analyzed were from three independent experiments.

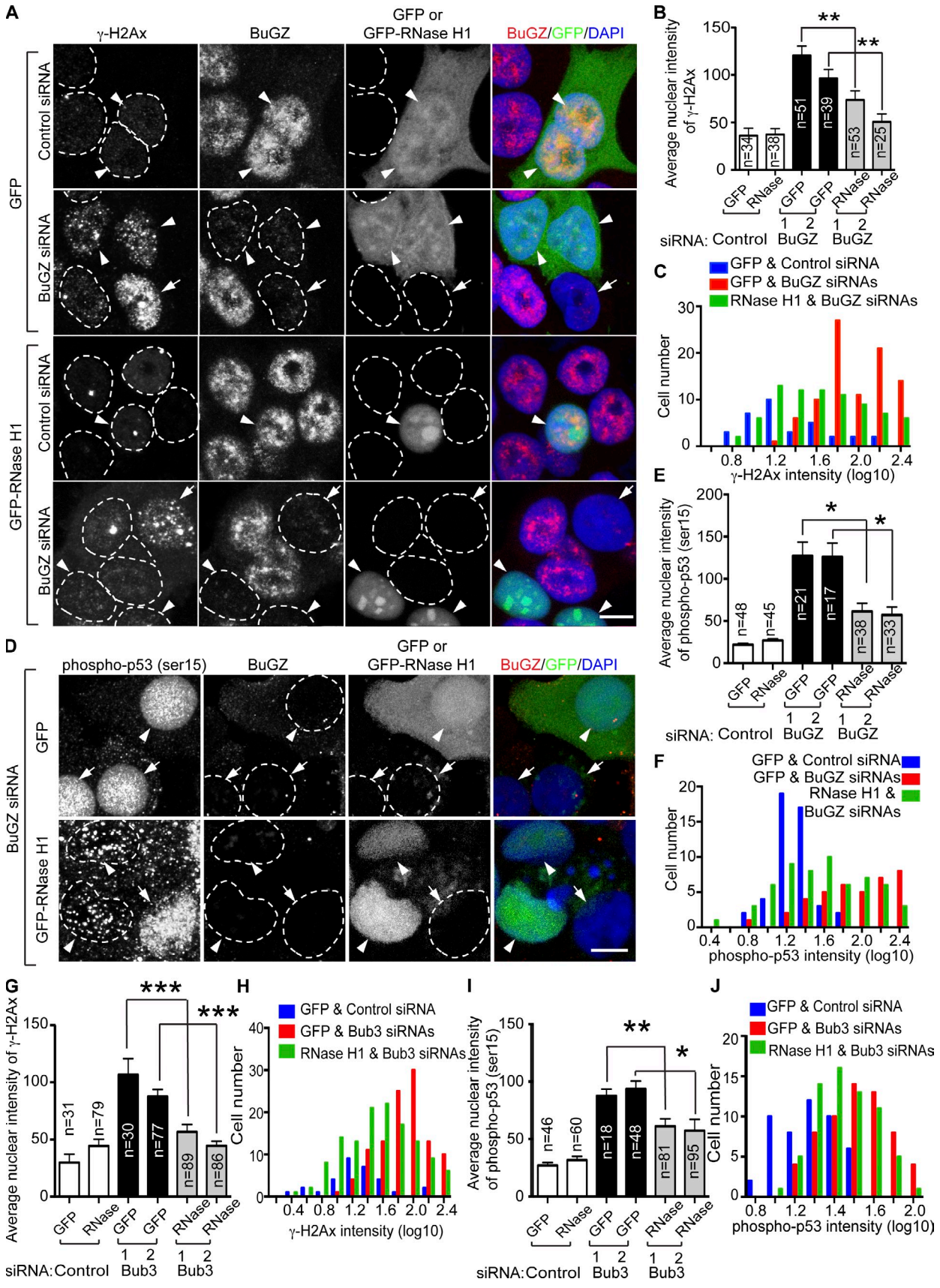

Figure 5. **Expression of RNase H1 in BuGZ- or Bub3-depleted HT29 cells reduces γ-H2Ax and phospho-p53 signals.** (A) GFP-RNase H1 (RNase), but not GFP, repressed BuGZ depletion-induced DNA damage in HT29 cells. Cells were first transfected by siRNAs for 12 h and then by GFP-RNase H1 or GFP plasmid for 48 h followed by immunofluorescence microscopy analyses. BuGZ-depleted cells with or without GFP fluorescence are indicated by arrowheads

used), and cell lines, please refer to Table S2. The plasmid for expressing GFP-RNase H1 was provided by R.J. Crouch (National Institute of Child Health and Human Development, Bethesda, MD).

Cell culture, plasmids, and siRNA transfection

For TOV21G cell (ATCC) culture, the base medium was a 1:1 mixture of MCDB 105 medium (Sigma-Aldrich) containing a final concentration of 1.5 g/liter sodium bicarbonate and Medium 199 (Sigma-Aldrich) containing a final concentration of 2.2 g/liter sodium bicarbonate. To make the complete growth medium, fetal bovine serum (Gibco) was added to a final concentration of 15%. HT29 (HTB-38; ATCC) and HeLa (CCL-2; ATCC) cells were cultured in Dulbecco's modified Eagle's medium (Gibco) containing 10% fetal bovine serum (Gibco) in 5% CO_2 at 37°C. The HFF cells (Millipore) were cultured in FibroGRO LS (low serum) Complete Medium (Millipore). HFFs were changed into fresh medium every other day and passaged using Accutase (Millipore) at a 1:3 dilution when reaching ∼80% of confluency.

The plasmids or siRNA transfections were performed using Lipofectamine 2000 (Life Technologies) or Lipofectamine RNAiMAX (Life Technologies), respectively. Cells were fixed for immunofluorescence analyses 48 h after siRNA transfection unless otherwise indicated. For cotransfection of siRNA and plasmids, siRNA was transfected first using the reverse transfection protocol. In brief, 10 pmol siRNA oligo was diluted in 50 µl Opti-MEM I Medium (Gibco) per well of a 24-well tissue culture plate. 1.5 µl of Lipofectamine RNAiMAX was added to each well. After mixing, the plate was incubated for 20 min at room temperature. Meanwhile, cells to be transfected were trypsinized and resuspended in complete growth medium without antibiotics. Cell suspension containing 20,000 cells was added into each well for transfection. After 24 h of transfection, cells were transfected with the indicated plasmids. For immunofluorescence analyses in Fig. 5, cells were fixed 48 h after plasmid transfection. For mitotic index calculation in Fig. S1, both tumor cells and primary cells were fixed at 60 h after RNAi followed by immunostaining. For FACS analysis of apoptotic cells in Fig. 1 and Fig. S1, both tumor cells and primary cells were analyzed 72 h after siRNA transfection.

FACS analyses of apoptotic cells

FITC Annexin V Apoptosis Detection kit with 7-AAD (640922; BioLegend) was used to detect apoptosis. 5×10^5 cells that were treated by control or BuGZ siRNAs (Fig. 1 B) were trypsinized and resuspended as individual cells in 100 µl of Annexin V–binding buffer (140 mM NaCl, 4 mM KCl, 0.75 mM $MgCl_2$, and 10 mM Hepes, pH 7.4). 5 µl FITC-Annexin V and 5 µl 7-AAD were added to each cell suspension. After incubation for 15 min at room temperature, cells were analyzed with FACS Aria III. For all samples, 100,000 events were recorded. FACSDIVA software (BD) was used for all flow cytometry analyses. Samples with buffer alone (background autofluorescence control), FITC-Annexin V, or 7-AAD staining alone (compensation controls for each fluorochrome) were used for compensation and gating for the apoptotic-positive cells. PE-Cy5 channel was used to detect 7-AAD fluorescence.

Immunofluorescence microscopy and quantifications

To detect DNA–RNA hybrids (R-loops) using the monoclonal antibody S9.6 (provided by L. Wahba and D. Koshland, University of California, Berkeley, Berkeley, CA; Phillips et al., 2013), we found that the treatment used for mitotic chromosome spread (Campos et al., 2009) improves the detection of R-loops in the nuclei of HT29 cells, whereas standard immunostaining was sufficient for HFFs. We modified the chromosome-spread method to treat the interphase HT29 cells. Control or siRNA-treated HT29 cells were trypsinized and resuspended as single cell suspensions and then treated with hypotonic solution (75 mM KCl) prewarmed to 37°C. The cells were then fixed with freshly made fixative solution (methanol/glacial acetic acid 3:1) overnight at 4°C. To spread the cells on a coverslip, the fixed cell suspension was placed on the coverslip exposed to the steam of hot water (90°C) for 30 s, which caused the cells to spread their chromatin on the coverslip. These cells were blocked by blocking buffer (5% BSA and 0.5% Triton X-100 in PBS) for 1 h and then incubated with 1:1,000 dilution of the S9.6 antibody overnight in blocking buffer. After three washes with blocking buffer, the cells were incubated with 1:1,000 dilution of secondary antibody for 1 h. For detection of R-loops in HFFs, cells were fixed using ice-cold methanol for 15 min followed by treatment with 70% ethanol for 15 min. Cells were washed three times with 70% ethanol for 5 min each followed by blocking and antibody staining as above.

For immunodetection of α-tubulin, γ-H2Ax, phospho-p53, BuGZ, and Bub3, cells grown on coverslips were fixed in 4% paraformaldehyde for 15 min and then permeabilized with 0.5% Triton X-100 in PBS for 5 min. The source and dilutions of the primary and secondary antibodies can be found in the Table S2.

To co-stain phospho-p53 and Bub3 with two mouse monoclonal antibodies (Table S2), the antibodies were directly coupled with Alexa Fluor 546 or Alexa Fluor 647, respectively, by using an APEX Alexa Fluor antibody labeling kit (A20183 and A20186; Life Technologies).

To detect GFP or GFP fusion proteins, cells were fixed in the same manner and imaged directly. After antibody staining and washes, the cells were stained with DAPI at 0.25 µg/ml in PBS for 5 min and mounted in Fluorescence Mounting medium (Dako).

Fluorescence images were captured using a microscope (ECLIPSE TE2000-U; Nikon) driven by MetaMorph software (Molecular Devices) or a laser confocal microscope (TCS SP5; Leica) at the same setting throughout each given experiment. For confocal microscopy, 63× 1.4 NA oil and 40× 1.25 NA oil objective lenses (Leica) were used and the cells were imaged by scanning optical sections at ∼0.5-µm intervals.

To quantify the mitotic index, the number of cells in prophase through telophase (judged by α-tubulin and DAPI staining) was divided by the total number of cells analyzed.

To quantify nuclear immunofluorescence intensity from confocal images, maximal projection was created from the z stacks for each nucleus. We used a method based on a previous study (King et al., 2000) to determine the nuclear fluorescence signal from both confocal images and images from epifluorescence microscopes. In brief, the nuclear regions (X) were defined by DAPI staining. A larger area surrounding the nucleus was then drawn (Y). Areas of X and Y were determined as Xa and Ya. The mean fluorescence intensity for X and Y were measured as Xf and Yf. Signal intensity for each nucleus (Xi) was determined as $Xi = Xf - (Yf \times Ya - Xf \times Xa)/(Ya - Xa)$.

All experiments were performed at least three times. A total of 17–159 nuclei were quantified from these experiments and plotted.

Senescence-associated (SA)-β-gal assay

We used the Senescence β-Galactosidase Staining kit (9860S; Cell Signaling) to detect β-galactosidase activity at pH 6.0. In brief, cells were fixed in the fixative solution for 10–15 min at room temperature. The fixed cells were then incubated with β-galactosidase staining solution containing X-gal at 37°C overnight. As the blue color developed, bright-field cell images were taken using an Axiovert 25 microscope (Carl Zeiss) connected to a Canon camera.

Live cell number count

A 0.4% Trypan blue stock solution (15250061; Life Technologies) was used to stain dead cells. 10 µl of Trypan blue stock solution was added to 100 µl of cell suspension. Cells negative for Trypan blue staining were counted as live cells using hemocytometer.

Immunoprecipitation and Western blotting analyses

To confirm the interaction between BuGZ or Bub3 and spliceosome components, we used two methods. In the first method, we transfected HEK293T cells with Flag-BuGZ, Flag-Bub3, or Flag-luciferase (negative control). After

or arrows, respectively. The broken lines indicate nuclear boundaries. Bar, 10 µm. (B and C) Quantifications for the mean fluorescence intensity of γ-H2Ax (B) and the intensity distributions (C) of the experiments shown in A. (D) GFP-RNase H1 repressed BuGZ depletion-induced p53 phosphorylation in HT29 cells. Arrowheads and arrows indicate cells with or without GFP-RNase H1, respectively. White broken circles outline the nuclei. (E and F) Quantifications for the mean fluorescence intensity of phospho-p53 (E) and the intensity distributions (F) of the experiments shown in D. (G and H) Quantifications for the mean fluorescence intensity of γ-H2Ax (G) and the intensity distributions (H) in Bub3-depleted and GFP- or GFP-RNase H1–expressing HT29 cells. (I and J) Quantifications for the mean fluorescence intensity of phospho-p53 (I) and the intensity distributions (J) in Bub3-depleted and GFP- or GFP-RNase H1–expressing HT29 cells. Error bars indicate SEM. Student's *t* test: *, $P < 0.05$; **, $P < 0.01$; ***, $P < 0.001$. Cell numbers (*n*) analyzed were from three independent experiments.

transfection, ~1 × 10^7 cells were lysed in 1 ml lysis buffer (20 mM Tris-Cl, pH 7.4, 150 mM KCl, 1 mM EDTA, 1 mM NaF, 1 mM DTT, 1% NP-40, 10% glycerol, and 1 mM sodium pyrophosphate) containing protease inhibitors (at 1 tablet/10 ml; cOmplete, Mini, EDTA-free, Protease Inhibitor Cocktail Tablets, 11836170001; Roche) at 4°C. After 10 min of centrifugation at 13,000 rpm in an Eppendorf tabletop centrifuge, the supernatant containing soluble proteins was incubated with a 30-µl slurry of anti-Flag M2 resin (A2220; Sigma-Aldrich) at 4°C for 4 h. After washing the beads with wash buffer (50 mM Tris-Cl, pH 7.4, 150 mM NaCl, 1 mM EDTA, 50 mM NaF, 1 mM DTT, and 1% NP-40) three times, the bound proteins were eluted with 100 µl Flag-peptide (F4799; Sigma-Aldrich) dissolved in the wash buffer at a concentration of 0.5 mg/ml.

In the second method, we used antibodies to BuGZ (HPA017013; Sigma-Aldrich), Bub3 (611731; BD), U2AF65 (ab37530; Abcam), Sf3a3 (ab156873; Abcam), or control IgG (12-370, 12-371; Millipore) to immunoprecipitate the respective endogenous proteins from HT29 cell lysates made from ~1 × 10^7 cells for each immunoprecipitation. Each antibody was preincubated with a 50-µl slurry of protein G Dynabeads (10007D; Life Technologies) for 30 min followed by washes with lysis buffer. The beads were added to the cell lysate and incubated overnight. The beads were then washed as described in the previous paragraph, and bound proteins were eluted with 100 µl of elution buffer (50 mM glycine at pH 2.5) and dissolved in the SDS sample buffer.

For Western blotting analyses of the Flag antibody immunoprecipitated proteins, 1% of input lysate and 10% of resuspended immunoprecipitates were loaded per lane for SDS-PAGE. Because the molecular weights of the proteins of BuGZ, U2AF65, and Sf3a3 are close to the heavy chain of IgG, we reduced the signal from the antibody heavy chain by using the secondary antibody specific to the rabbit light chain (211-032-171; Jackson ImmunoResearch Laboratories, Inc.). Flag (F3165; Sigma-Aldrich), BuGZ (HPA017013; Sigma-Aldrich), Bub3 (611731; BD), U2AF65 (ab37530; Abcam), or Sf3a3 (ab156873; Abcam) antibodies were used at the indicated dilutions (Table S2).

Whole-transcriptome shotgun sequencing (RNA-Seq) and data analyses

Arcturus PicoPure RNA isolation kit (KIT0204; Life Technologies) was used to prepare total RNA from cells. Ribo-Zero Gold kits (human/mouse/rat; MRZG126; Epicentre) were used to remove both cytoplasmic (nuclear-encoded) rRNA and mitochondrial rRNA from total RNA preparations, and libraries were built using the Illumina TruSeq RNA sample prep kit V2 (RS-122-2001; Illumina). Libraries were sequenced using an Illumina HiSeq 2000. Single-end 100-bp reads were obtained.

RNA-Seq reads were first mapped to the human genome (hg19) using Tophat2 (Kim et al., 2013). Transcript annotation from Ensembl was used as reference for exon junctions in read mapping. We then used Cufflinks (Trapnell et al., 2010, 2012; Pollier et al., 2013) to assemble unannotated transcripts. Assembled transcripts from the same cell type were further merged by Cuffmerge (Trapnell et al., 2010). Finally, we used MATS (Shen et al., 2012; Park et al., 2013) to call differential alternative splicing, and the merged transcripts from the previous step were used as transcript annotation in MATS.

Drosophila stocks

The w^{1118} allele (Bloomington Drosophila Stock Center no. 3605) was used as the wild-type control. The RNAi strains for *BuGZ* were obtained from the Vienna Drosophila RNAi library: w^{1118}; P{GD9485}v45449 (Vienna Drosophila Resource Center no. v45449). dsRNA-GD9485 (2L:16,744,705 ... 16,745,060) was inserted in the third chromosome.

The *UAS* strains used were: *UAS-upd* transgenic fly generated through transformation of *UAS-upd* construct into W^{1118} flies by standard methods (provided by X. Chen, Johns Hopkins University, Baltimore, MD; Kiger et al., 2001) and *UAS-yki*$^{S111A.S168A.S250A.V5}$ (Bloomington Drosophila Stock Center no. 28817). The *Gal4* allele used to drive the *UAS* lines is *ey-Gal4* (Bloomington Drosophila Stock Center no. 5534), which is expressed in the *Drosophila* eyes.

Drosophila genetics and culture

If not specifically mentioned, all the flies were maintained on standard cornmeal/molasses/yeast fly food (the recipe for 1 liter of food: 50 g cornmeal, 18.75 g yeast, 5 g agar, 62.5 ml molasses, 11.5 ml 5% anti-fungal agent Tegosept, and 35 ml propionic acid). Flies were cultured at 25°C on a normal light/dark cycle condition, unless otherwise indicated.

To induce the tumor formation in the *Drosophila* eyes, *ey-Gal4* was used to drive oncogene expression specifically in the eye. *UAS-upd* and *UAS-yki*$^{S111A.S168A.S250A.V5}$ transgenic flies were used to generate eye tumors.

To investigate the tumor repression effect of *BuGZ* RNAi, we used *ey-Gal4* to drive both *UAS-upd* (or *UAS-yki*$^{S111A.S168A.S250A.V5}$) and *UAS-BuGZ RNAi*. The crosses were set up at 25°C, and eye tumor formation was examined after eclosion.

To evaluate the tumor repression effect of the splicing inhibitor pladienolide B, *ey-Gal4>UAS-upd* (or *UAS-yki*$^{S111A.S168A.S250A.V5}$) flies were fed with DMSO/pladienolide B (5 µM) from the first instar larval stage. Eye tumor formation was examined after eclosion.

To quantify the area of each *Drosophila* eye, bright-field images of the eyes were taken by placing the fly's head dorsal-side-up under a stereomicroscope (SMZ1500; Nikon) with a camera (AxioCam HRC; Carl Zeiss). This allows us to visualize the contour and half of the total area of the fly eyes. The rough eyes have a rough contour and a larger area than normal eyes, which are quantified by measuring the pixel number in each eye area using Photoshop CS5 (Adobe).

To investigate the RNAi knockdown efficiency of the *UAS-BuGZ* RNAi allele, *tub*-Gal4 (Bloomington Drosophila Stock Center no. 5138) was used to drive the ubiquitous expression of *UAS-BuGZ RNAi*, with the *UAS-LacZ RNAi* allele as the control. Total RNAs were collected at either the third instar larval stage or pupal stage, and qRT-PCR was performed to examine the mRNA level of *BuGZ*.

Scanning EM

Drosophila heads were excised and placed in McDowell's and Trump's 4F:1G (McDowell and Trump, 1976) fixative for 1 h to several weeks at 4°C. After two rinses in 0.1 M sodium phosphate buffer (pH 7.2), samples were dehydrated in a graded ethanol series to 100% ethanol, at which time they were critical point-dried with liquid CO_2. Finally, they were mounted on specimen stubs with colloidal silver, sputter-coated with gold-palladium, and examined with a scanning electron microscope (Quanta 200 Environmental Scanning Electron Microscope; FEI).

Quantitative real-time PCR

Total RNA was isolated from *Drosophila* larvae or pupae using an RNA isolation kit (RNeasy Plus Mini kit; QIAGEN) and the manufacturer's protocol. Quantitative RT-PCR was performed using the iScript One Step RT-PCR kit (170-8892; Bio-Rad Laboratories) on a real-time PCR detection system (CFX96; Bio-Rad Laboratories). 50 ng of total RNA was reverse transcribed and amplified as follows: 50°C for 10 min, 95°C for 5 min, 95°C for 10 s, 60°C for 30 s, 72°C for 1 min. Steps 2–4 were repeated for 40 cycles. Each reaction was performed in triplicate, and the results of three independent experiments were used for statistical analysis. Relative mRNA expression levels were quantified using the ΔΔC(t) method (Pfaffl, 2001). Results were normalized to those for RP49, and primer sequences were as follows. Rp49 (*Drosophila*): forward primer, TACAGGCCCAAGATCGTGAA; and reverse primer, TCTCCTTGCGCTTCTTGGA. BuGZ (*Drosophila*): forward primer, AAGCCACCTTAGGATCATGG; and reverse primer, GGGTCCGGTGTACAACTTCT.

Online supplemental material

Fig. S1 shows the effect of BuGZ reduction on the mitotic index and cell proliferation. Fig. S2 shows the tumor repression effect of BuGZ RNAi or pladienolide B treatment. Fig. S3 shows that DNA damage caused by splicing inhibitor treatment can be rescued by forced expression of RNase H1. Table S1 gives a list of differential alternative splicing events caused by BuGZ RNAi, Bub3 RNAi, or pladienolide B treatment. Table S2 gives the sources and sequences of mammalian expression plasmids, antibodies (with dilutions used), siRNA, shRNA, small molecules (with concentrations used), and cell lines. Online supplemental material is available at http://www.jcb.org/cgi/content/full/jcb.201409073/DC1. Additional data are available in the JCB DataViewer at http://dx.doi.org/10.1083/jcb.201409073.dv.

We thank the members of the Zhu and Zheng laboratories for comments and technical help, Dr. R.J. Crouch for the GFP-RNase H1 plasmid, Drs. Lamia Wahba and Doug Koshland for the S9.6 antibody, and Allison Pinder for RNA-Seq.

This paper was supported by the Chinese Academy of Sciences (XDA01010107 to X. Zhu), the Ministry of Science and Technology of China (2014CB964803 to X. Zhu), the National Science Foundation of China (31420103916 to X. Zhu and Y. Zheng), and NIH/NIGMS grants R01 GM056312 (to Y. Zheng), and R01 GM06023 (to Y. Zheng).

The authors declare no competing financial interests.

Submitted: 15 September 2014
Accepted: 12 March 2015

References

Aguilera, A., and T. García-Muse. 2012. R loops: from transcription byproducts to threats to genome stability. *Mol. Cell*. 46:115–124. http://dx.doi.org/10.1016/j.molcel.2012.04.009

Blagosklonny, M.V. 2006. Prolonged mitosis versus tetraploid checkpoint: how p53 measures the duration of mitosis. *Cell Cycle*. 5:971–975. http://dx.doi.org/10.4161/cc.5.9.2711

Campisi, J., and F. d'Adda di Fagagna. 2007. Cellular senescence: when bad things happen to good cells. *Nat. Rev. Mol. Cell Biol.* 8:729–740. http://dx.doi.org/10.1038/nrm2233

Campos, P.B., R.C. Sartore, S.N. Abdalla, and S.K. Rehen. 2009. Chromosomal spread preparation of human embryonic stem cells for karyotyping. *J. Vis. Exp.* 31:1512.

Cerritelli, S.M., E.G. Frolova, C. Feng, A. Grinberg, P.E. Love, and R.J. Crouch. 2003. Failure to produce mitochondrial DNA results in embryonic lethality in Rnaseh1 null mice. *Mol. Cell*. 11:807–815. http://dx.doi.org/10.1016/S1097-2765(03)00088-1

Chen, Q.M., J.B. Merrett, T. Dilley, and S. Purdom. 2002. Down regulation of p53 with HPV E6 delays and modifies cell death in oxidant response of human diploid fibroblasts: an apoptosis-like cell death associated with mitosis. *Oncogene*. 21:5313–5324. http://dx.doi.org/10.1038/sj.onc.1205644

Drolet, M., P. Phoenix, R. Menzel, E. Massé, L.F. Liu, and R.J. Crouch. 1995. Overexpression of RNase H partially complements the growth defect of an *Escherichia coli* delta topA mutant: R-loop formation is a major problem in the absence of DNA topoisomerase I. *Proc. Natl. Acad. Sci. USA*. 92:3526–3530. http://dx.doi.org/10.1073/pnas.92.8.3526

Effenberger, K.A., R.J. Perriman, W.M. Bray, R.S. Lokey, M. Ares Jr., and M.S. Jurica. 2013. A high-throughput splicing assay identifies new classes of inhibitors of human and yeast spliceosomes. *J. Biomol. Screen.* 18:1110–1120. http://dx.doi.org/10.1177/1087057113493117

Eskens, F.A., F.J. Ramos, H. Burger, J.P. O'Brien, A. Piera, M.J. de Jonge, Y. Mizui, E.A. Wiemer, M.J. Carreras, J. Baselga, and J. Tabernero. 2013. Phase I pharmacokinetic and pharmacodynamic study of the first-in-class spliceosome inhibitor E7107 in patients with advanced solid tumors. *Clin. Cancer Res.* 19:6296–6304. http://dx.doi.org/10.1158/1078-0432.CCR-13-0485

Forbes, S.A., N. Bindal, S. Bamford, C. Cole, C.Y. Kok, D. Beare, M. Jia, R. Shepherd, K. Leung, A. Menzies, et al. 2011. COSMIC: mining complete cancer genomes in the Catalogue of Somatic Mutations in Cancer. *Nucleic Acids Res.* 39(Database):D945–D950. http://dx.doi.org/10.1093/nar/gkq929

Gan, W., Z. Guan, J. Liu, T. Gui, K. Shen, J.L. Manley, and X. Li. 2011. R-loop-mediated genomic instability is caused by impairment of replication fork progression. *Genes Dev.* 25:2041–2056. http://dx.doi.org/10.1101/gad.17010011

Ganem, N.J., and D. Pellman. 2012. Linking abnormal mitosis to the acquisition of DNA damage. *J. Cell Biol.* 199:871–881. http://dx.doi.org/10.1083/jcb.201210040

Gascoigne, K.E., and S.S. Taylor. 2008. Cancer cells display profound intra- and interline variation following prolonged exposure to antimitotic drugs. *Cancer Cell*. 14:111–122. http://dx.doi.org/10.1016/j.ccr.2008.07.002

Gonzalez, C. 2013. *Drosophila melanogaster*: a model and a tool to investigate malignancy and identify new therapeutics. *Nat. Rev. Cancer*. 13:172–183. http://dx.doi.org/10.1038/nrc3461

Groh, M., M.M. Lufino, R. Wade-Martins, and N. Gromak. 2014. R-loops associated with triplet repeat expansions promote gene silencing in Friedreich ataxia and fragile X syndrome. *PLoS Genet.* 10:e1004318. http://dx.doi.org/10.1371/journal.pgen.1004318

Hayashi, M.T., A.J. Cesare, J.A. Fitzpatrick, E. Lazzerini-Denchi, and J. Karlseder. 2012. A telomere-dependent DNA damage checkpoint induced by prolonged mitotic arrest. *Nat. Struct. Mol. Biol.* 19:387–394. http://dx.doi.org/10.1038/nsmb.2245

Hegele, A., A. Kamburov, A. Grossmann, C. Sourlis, S. Wowro, M. Weimann, C.L. Will, V. Pena, R. Lührmann, and U. Stelzl. 2012. Dynamic protein-protein interaction wiring of the human spliceosome. *Mol. Cell*. 45:567–580. http://dx.doi.org/10.1016/j.molcel.2011.12.034

Huang, H.C., J. Shi, J.D. Orth, and T.J. Mitchison. 2010. Cell death when the SAC is out of commission. *Cell Cycle*. 9:2049–2050. http://dx.doi.org/10.4161/cc.9.11.11918

Inuzuka, H., S. Shaik, I. Onoyama, D. Gao, A. Tseng, R.S. Maser, B. Zhai, L. Wan, A. Gutierrez, A.W. Lau, et al. 2011. SCF(FBW7) regulates cellular apoptosis by targeting MCL1 for ubiquitylation and destruction. *Nature*. 471:104–109. http://dx.doi.org/10.1038/nature09732

Ismail, N., A.H. Pihie, and M. Nallapan. 2005. Xanthorrhizol induces apoptosis via the up-regulation of bax and p53 in HeLa cells. *Anticancer Res.* 25(3B):2221–2227.

Jiang, H., X. He, S. Wang, J. Jia, Y. Wan, Y. Wang, R. Zeng, J. Yates III, X. Zhu, and Y. Zheng. 2014. A microtubule-associated zinc finger protein, BuGZ, regulates mitotic chromosome alignment by ensuring Bub3 stability and kinetochore targeting. *Dev. Cell*. 28:268–281. http://dx.doi.org/10.1016/j.devcel.2013.12.013

Khoo, K.H., C.S. Verma, and D.P. Lane. 2014. Drugging the p53 pathway: understanding the route to clinical efficacy. *Nat. Rev. Drug Discov.* 13:217–236. (published erratum appears in *Nat. Rev. Drug Discov.* 13:314) http://dx.doi.org/10.1038/nrd4236

Kiger, A.A., D.L. Jones, C. Schulz, M.B. Rogers, and M.T. Fuller. 2001. Stem cell self-renewal specified by JAK-STAT activation in response to a support cell cue. *Science*. 294:2542–2545. http://dx.doi.org/10.1126/science.1066707

Kim, D., G. Pertea, C. Trapnell, H. Pimentel, R. Kelley, and S.L. Salzberg. 2013. TopHat2: accurate alignment of transcriptomes in the presence of insertions, deletions and gene fusions. *Genome Biol.* 14:R36. http://dx.doi.org/10.1186/gb-2013-14-4-r36

King, J.M., T.S. Hays, and R.B. Nicklas. 2000. Dynein is a transient kinetochore component whose binding is regulated by microtubule attachment, not tension. *J. Cell Biol.* 151:739–748.

Komarov, P.G., E.A. Komarova, R.V. Kondratov, K. Christov-Tselkov, J.S. Coon, M.V. Chernov, and A.V. Gudkov. 1999. A chemical inhibitor of p53 that protects mice from the side effects of cancer therapy. *Science*. 285:1733–1737. http://dx.doi.org/10.1126/science.285.5434.1733

Kotake, Y., K. Sagane, T. Owa, Y. Mimori-Kiyosue, H. Shimizu, M. Uesugi, Y. Ishihama, M. Iwata, and Y. Mizui. 2007. Splicing factor SF3b as a target of the antitumor natural product pladienolide. *Nat. Chem. Biol.* 3:570–575. http://dx.doi.org/10.1038/nchembio.2007.16

Lanni, J.S., and T. Jacks. 1998. Characterization of the p53-dependent postmitotic checkpoint following spindle disruption. *Mol. Cell. Biol.* 18:1055–1064.

Li, X., and J.L. Manley. 2005. Inactivation of the SR protein splicing factor ASF/SF2 results in genomic instability. *Cell*. 122:365–378. http://dx.doi.org/10.1016/j.cell.2005.06.008

Lin, Y., S.Y. Dent, J.H. Wilson, R.D. Wells, and M. Napierala. 2010. R loops stimulate genetic instability of CTG·CAG repeats. *Proc. Natl. Acad. Sci. USA*. 107:692–697. http://dx.doi.org/10.1073/pnas.0909740107

McDowell, E.M., and B.F. Trump. 1976. Histologic fixatives suitable for diagnostic light and electron microscopy. *Arch. Pathol. Lab. Med.* 100:405–414.

Orth, J.D., A. Loewer, G. Lahav, and T.J. Mitchison. 2012. Prolonged mitotic arrest triggers partial activation of apoptosis, resulting in DNA damage and p53 induction. *Mol. Biol. Cell*. 23:567–576. http://dx.doi.org/10.1091/mbc.E11-09-0781

Park, J.W., C. Tokheim, S. Shen, and Y. Xing. 2013. Identifying differential alternative splicing events from RNA sequencing data using RNASeq-MATS. *Methods Mol. Biol.* 1038:171–179. http://dx.doi.org/10.1007/978-1-62703-514-9_10

Paulsen, R.D., D.V. Soni, R. Wollman, A.T. Hahn, M.C. Yee, A. Guan, J.A. Hesley, S.C. Miller, E.F. Cromwell, D.E. Solow-Cordero, et al. 2009. A genome-wide siRNA screen reveals diverse cellular processes and pathways that mediate genome stability. *Mol. Cell*. 35:228–239. http://dx.doi.org/10.1016/j.molcel.2009.06.021

Pfaffl, M.W. 2001. A new mathematical model for relative quantification in real-time RT-PCR. *Nucleic Acids Res.* 29:e45. http://dx.doi.org/10.1093/nar/29.9.e45

Phillips, D.D., D.N. Garboczi, K. Singh, Z. Hu, S.H. Leppla, and C.E. Leysath. 2013. The sub-nanomolar binding of DNA-RNA hybrids by the single-chain Fv fragment of antibody S9.6. *J. Mol. Recognit.* 26:376–381. http://dx.doi.org/10.1002/jmr.2284

Pilch, D.R., O.A. Sedelnikova, C. Redon, A. Celeste, A. Nussenzweig, and W.M. Bonner. 2003. Characteristics of γ-H2AX foci at DNA double-strand breaks sites. *Biochem. Cell Biol.* 81:123–129. http://dx.doi.org/10.1139/o03-042

Pollier, J., S. Rombauts, and A. Goossens. 2013. Analysis of RNA-Seq data with TopHat and Cufflinks for genome-wide expression analysis of jasmonate-treated plants and plant cultures. *Methods Mol. Biol.* 1011:305–315. http://dx.doi.org/10.1007/978-1-62703-414-2_24

Porameesanaporn, Y., W. Uthaisang-Tanechpongtamb, F. Jarintanan, S. Jongrungruangchok, and B. Thanomsub Wongsatayanon. 2013. Terrein induces apoptosis in HeLa human cervical carcinoma cells through p53 and ERK regulation. *Oncol. Rep.* 29:1600–1608.

Quignon, F., L. Rozier, A.M. Lachages, A. Bieth, M. Simili, and M. Debatisse. 2007. Sustained mitotic block elicits DNA breaks: one-step alteration of ploidy and chromosome integrity in mammalian cells. *Oncogene*. 26:165–172. http://dx.doi.org/10.1038/sj.onc.1209787

Sato, M., N. Muguruma, T. Nakagawa, K. Okamoto, T. Kimura, S. Kitamura, H. Yano, K. Sannomiya, T. Goji, H. Miyamoto, et al. 2014. High antitumor

activity of pladienolide B and its derivative in gastric cancer. *Cancer Sci.* 105:110–116. http://dx.doi.org/10.1111/cas.12317

Scheffner, M., B.A. Werness, J.M. Huibregtse, A.J. Levine, and P.M. Howley. 1990. The E6 oncoprotein encoded by human papillomavirus types 16 and 18 promotes the degradation of p53. *Cell*. 63:1129–1136. http://dx.doi.org/10.1016/0092-8674(90)90409-8

Shen, S., J.W. Park, J. Huang, K.A. Dittmar, Z.X. Lu, Q. Zhou, R.P. Carstens, and Y. Xing. 2012. MATS: a Bayesian framework for flexible detection of differential alternative splicing from RNA-Seq data. *Nucleic Acids Res.* 40:e61. http://dx.doi.org/10.1093/nar/gkr1291

Song, G., Y.B. Mao, Q.F. Cai, L.M. Yao, G.L. Ouyang, and S.D. Bao. 2005. Curcumin induces human HT-29 colon adenocarcinoma cell apoptosis by activating p53 and regulating apoptosis-related protein expression. *Braz. J. Med. Biol. Res.* 38:1791–1798. http://dx.doi.org/10.1590/S0100-879X2005001200007

Stähler, F., and K. Roemer. 1998. Mutant p53 can provoke apoptosis in p53-deficient Hep3B cells with delayed kinetics relative to wild-type p53. *Oncogene*. 17:3507–3512. http://dx.doi.org/10.1038/sj.onc.1202245

Surova, O., and B. Zhivotovsky. 2013. Various modes of cell death induced by DNA damage. *Oncogene*. 32:3789–3797. http://dx.doi.org/10.1038/onc.2012.556

Toledo, C.M., J.A. Herman, J.B. Olsen, Y. Ding, P. Corrin, E.J. Girard, J.M. Olson, A. Emili, J.G. DeLuca, and P.J. Paddison. 2014. BuGZ is required for Bub3 stability, Bub1 kinetochore function, and chromosome alignment. *Dev. Cell*. 28:282–294. http://dx.doi.org/10.1016/j.devcel.2013.12.014

Trapnell, C., B.A. Williams, G. Pertea, A. Mortazavi, G. Kwan, M.J. van Baren, S.L. Salzberg, B.J. Wold, and L. Pachter. 2010. Transcript assembly and quantification by RNA-Seq reveals unannotated transcripts and isoform switching during cell differentiation. *Nat. Biotechnol.* 28:511–515. http://dx.doi.org/10.1038/nbt.1621

Trapnell, C., A. Roberts, L. Goff, G. Pertea, D. Kim, D.R. Kelley, H. Pimentel, S.L. Salzberg, J.L. Rinn, and L. Pachter. 2012. Differential gene and transcript expression analysis of RNA-seq experiments with TopHat and Cufflinks. *Nat. Protoc.* 7:562–578. http://dx.doi.org/10.1038/nprot.2012.016

Uetake, Y., and G. Sluder. 2010. Prolonged prometaphase blocks daughter cell proliferation despite normal completion of mitosis. *Curr. Biol.* 20:1666–1671. http://dx.doi.org/10.1016/j.cub.2010.08.018

Wahba, L., J.D. Amon, D. Koshland, and M. Vuica-Ross. 2011. RNase H and multiple RNA biogenesis factors cooperate to prevent RNA:DNA hybrids from generating genome instability. *Mol. Cell*. 44:978–988. http://dx.doi.org/10.1016/j.molcel.2011.10.017

Wahl, M.C., C.L. Will, and R. Lührmann. 2009. The spliceosome: design principles of a dynamic RNP machine. *Cell*. 136:701–718. http://dx.doi.org/10.1016/j.cell.2009.02.009

Wertz, I.E., S. Kusam, C. Lam, T. Okamoto, W. Sandoval, D.J. Anderson, E. Helgason, J.A. Ernst, M. Eby, J. Liu, et al. 2011. Sensitivity to antitubulin chemotherapeutics is regulated by MCL1 and FBW7. *Nature*. 471:110–114. http://dx.doi.org/10.1038/nature09779

Wimberly, H., C. Shee, P.C. Thornton, P. Sivaramakrishnan, S.M. Rosenberg, and P.J. Hastings. 2013. R-loops and nicks initiate DNA breakage and genome instability in non-growing Escherichia coli. *Nat. Commun.* 4:2115. http://dx.doi.org/10.1038/ncomms3115

Wongsurawat, T., P. Jenjaroenpun, C.K. Kwoh, and V. Kuznetsov. 2012. Quantitative model of R-loop forming structures reveals a novel level of RNA-DNA interactome complexity. *Nucleic Acids Res.* 40:e16. http://dx.doi.org/10.1093/nar/gkr1075